Chinese Chemical Letters 37 (2026) 111117

Contents lists available at ScienceDirect

Chinese Chemical Letters

journal homepage: www.elsevier.com/locate/cclet

Self-assembled supramolecular nanofibers integrate pH-responsive drug delivery and antimicrobial for combined cancer therapy

Ting Zhang[a,e,1,*], Deqiang Chen[e,1], Ningzhi Zhang[e], Mingxu Zhang[e], Qiang Huang[a,e], Wei Liu[a,e], Ran Gao[e], Yong Zhang[a,b,c,d,*]

[a] State Key Laboratory of Frigid Zone Cardiovascular Diseases (SKLFZCD), Department of Pharmacology, College of Pharmacy, Harbin Medical University, Harbin 150081, China
[b] Department of Cardiology, the Second Affiliated Hospital, Harbin Medical University, Harbin 150081, China
[c] State Key Laboratory-Province Key Laboratories of Biomedicine-Pharmaceutics of China, and Key Laboratory of Cardiovascular Research, Ministry of Education, College of Pharmacy, Harbin Medical University, Harbin 150081, China
[d] Research Unit of Noninfectious Chronic Diseases in Frigid Zone (2019RU070), Chinese Academy of Medical Sciences, Harbin 150081, China
[e] Department of Inorganic Chemistry and Physical Chemistry, College of Pharmacy, Harbin Medical University, Harbin 150081, China

ARTICLE INFO

Article history:
Received 10 January 2025
Revised 18 March 2025
Accepted 19 March 2025
Available online 20 March 2025

Keywords:
pH-responsive self-assembly nanofibers
Supramolecular interaction
Sequential release
Antibacterial
Combination therapy

ABSTRACT

Constructing nanofibers with specific therapeutic effects against cancer is a challenge. Here, we present the synthesis approach and application prospects of supramolecular nanofibers, which are based on cucurbit[8]uril (CB[8]) as the host and terpyridine lanthanum ions metal complex as the guest, constructed by layer-by-layer self-assembly through supramolecular interaction. Moreover, nanofibers with lanthanide luminescence properties exhibit surprising pH-responsive deformation properties and antibacterial behavior. In the tumor micro-environment, the dramatic reduction in the size of the nanofibers enables specific and hierarchical release of anticancer drugs in tumor cells to exert an advanced therapeutic effect. In addition, the synergistic therapeutic efficacy was achieved by reducing the excess of Gram-positive and Gram-negative bacteria surrounding tumor cells. The novel supramolecular nanofibers with sequential drug release and combined therapeutic mode provide new guidance for the synthesis of drug carrier materials and direction for the promotion of nanomaterial-mediated cancer therapy.

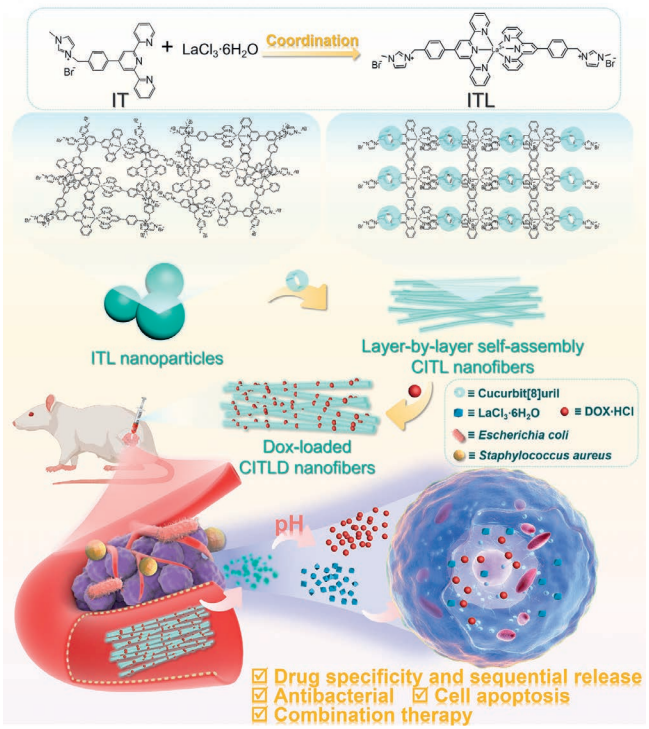
© 2025 Published by Elsevier B.V. on behalf of Chinese Chemical Society and Institute of Materia Medica, Chinese Academy of Medical Sciences.

In cancer treatment, chemotherapy is one of the most commonly used clinical treatment modalities. However, chemotherapeutic drugs can produce various adverse reactions in the human body, and how to avoid the damage of chemotherapy to normal cells or tissues, and design drug systems that respond to cancer cells have attracted extensive attention in medicine and chemistry [1]. Nanodelivery systems are one of the feasible pathways to solve the above problems [2–5], and there are many materials used as drug carriers, such as metal nanoparticles, mesoporous silica, liposomes, polymeric micelles, proteins, hydrogels and exosomes, among which nanofibers with large specific surface area, high drug loading rate, low toxicity, and degradability, and are therefore widely used in sustained release systems [6–13]. However, the traditional nanofibers preparation method has the disadvantages of high instrument conditions, single performance and high toxicity, *etc*., which limits the clinical application and transformation. Therefore, the development of structurally regulated nanofibers is currently challenging.

Supramolecular chemistry is an emerging interdisciplinary discipline that focuses on the formation of complex and ordered assemblies of molecules under non-covalent forces, providing methods and techniques for the synthesis and construction of new materials [14–20]. The utilization of supramolecular interaction to form nanofibers is an effective method that has attracted much attention in recent years. Compared with conventional polymers, each monomer in supramolecular polymers is assembled by non-covalent interactions, such as ionic interactions, hydrogen bonding, host-guest interactions, hydrophobic interactions, and van der Wal forces [21–24]. Liu and colleagues combined targeted peptide-encapsulated magnetic nanoparticles with polysaccharides containing β-cyclodextrins to construct supramolecular nanofibers with reversible morphology conversion triggered by a magnetic field for the treatment of tumors [25]. Li *et al.* jointly assembled supramolecular nanofibers with the immunomodulator thymopeptide and the near-infrared dye indocyanine green

* Corresponding authors.
E-mail addresses: tingzhang@hrbmu.edu.cn (T. Zhang), hmuzhangyong@hotmail.com (Y. Zhang).
[1] These authors contributed equally to this work.

https://doi.org/10.1016/j.cclet.2025.111117
1001-8417/© 2025 Published by Elsevier B.V. on behalf of Chinese Chemical Society and Institute of Materia Medica, Chinese Academy of Medical Sciences.



Scheme 1. Illustration schematic of synthetic route and cancer treatment process of layer-by-layer self-assembly supramolecular nanofibers.

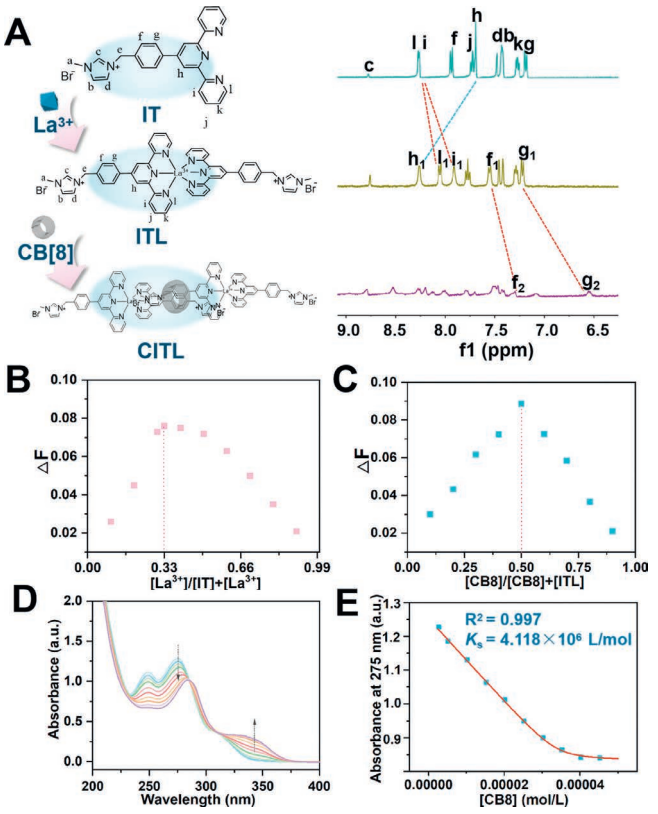


Fig. 1. (A) The ^{1}H NMR spectra (400 MHz, D_2O, 298 K) of 1.00 mmol/L of IT, ITL and CITL. (B) Job's plot for IT with La^{3+}. (C) Job's plot for CB[8] with ITL. (D, E) UV–vis spectra titration curve and the nonlinear least-squares analysis of ITL upon addition of CB[8].

for localized photo-thermal responsive immunotherapy of pancreatic tumors [26]. As a result, the nanofibers constructed based on supramolecular interactions not only have the structural properties of nanofibers, but also can overcome the sensitivity bottleneck caused by covalent interactions, satisfy the requirement of rapid response of the environment to external stimuli, and achieve controllable dynamic reversibility in different environments.

The tumor microenvironment (TME) is intimately related to tumor development, growth and metastasis [27–33]. Compared with the normal cellular microenvironment, the TME often exhibits hypoxia, acidification, inflammatory reactivity, and immunosuppression. In addition, recent studies have found that the intratumor microbial environment potentially promotes tumorigenesis and progression by inducing genomic instability and mutations, influencing epigenetic modifications, promoting inflammatory responses, averting immune destruction, regulating metabolism, and activating invasion and metastasis [34–36]. However, the traditional single antibacterial agents such as antibiotics and other drugs have an obvious effect on the treatment of bacteria, but the treatment effect on tumors is poor. Due to the lack of targeting, systemic dose administration of antibiotics can induce a series of negative effects, including disruption of microbiome balance, drug resistance, and susceptibility to infection, especially for patients with malignant tumors [37–39]. Recently, Yu *et al.* have addressed increased immunosuppression and tumor overgrowth in breast and prostate cancer by combining antimicrobial agents with antitumor therapy [40]. Therefore, interventions to establish modulation of the intratumor microbiota on top of conventional treatments show great potential to open a new chapter in antitumor therapy.

Here, supramolecular nanofibers based on cucurbituril/terpyridine (Tpy) derivatives/lanthanide ions (La^{3+}) were constructed and studied for tumor therapy. Cucurbit[8]uril (CB[8]) was chosen as the main body of supramolecular nanofibers because of its strong selectivity, specificity and affinity, which has a wide range of chemistry, biology, material and physics. As shown in Scheme 1, *n*-methylimidazole-modified terpyridine (IT) was designed and synthesized as the guest molecule. Not only can Tpy complex with biomolecules become an active molecule of valid anticancer drugs, but also by Tpy with La^{3+} that inhibit the growth effect of cancer cells in metal coordination to obtain ITL complexes, showing lanthanide luminescence. The chelation of Tpy with rare-earth ions (La^{3+}) under metal coordination not only exhibited lanthanide luminescence, but the anticancer effect of La^{3+} made the Im-Tpy/La^{3+} (ITL) complex a potential candidate for tumor cell inhibition. The imidazole cation at the other end of IT acted as a guest molecule and bound to the main molecule CB[8] based on the host-guest interaction, then self-assembled into supramolecular nanofibers. Interestingly, we found that the nanofibers exhibited rapid deformation under a slight change in pH and lanthanide luminescence performance, which was a great advantage for specific anticancer therapy. When regarded as nanocarriers, the nanofibers loaded with drugs enable decomposition hierarchically in the TME and play the controllable release function. More importantly, the multifunctional antibacterial behavior of nanofibers has potential applications in cancer treatment and metastasis inhibition. This work proposed an approach for drug carrier design and application by constructing multifunctional supramolecular nanofibers through layer-by-layer self-assembly, which opened up innovative insights for cancer.

IT was synthesized according to our previously published literature [15]. As shown in Fig. 1A, the nuclear magnetic resonance hydrogen spectroscopy (^{1}H NMR) spectra proved the successful synthesis of the IT compound. The bonding ratio of IT and $LaCl_3{\cdot}6H_2O$ was determined by the change of ultraviolet-visible spectroscopy (UV–vis) absorption spectra, as seen in Fig. 1B, in $CHCl_3/CH_3CN$ (v/v, 1:1) solution, the sum of host and guest concentrations was 0.05 mmol/L. Taking the value of the absorption change of IT at

275 nm as the vertical coordinate, when the $[La^{3+}]/[IT]+[La^{3+}]$ ratio was 0.33, the absorption change reached the highest, proving that IT was assembled with La^{3+} in a 2:1 stoichiometric ratio. In addition, ^1H NMR was used to investigate the mode of host and guest. IT and $LaCl_3{\cdot}6H_2O$ were mixed in a 2:1 molar ratio, and as shown in Fig. 1A, the shifts of protons H_l and H_i on the aromatic ring of the Tpy in IT compound shifted toward the high field, while the H_h showed a slight downfield shifted and accompanied by significant passivation. The above results indicated that IT with La^{3+} formed a stable metal complex ITL under coordination interaction.

Further, the macrocyclic molecule CB[8] was introduced to interact with the metal complex ITL for secondary assembly, and the methylimidazole cationic group of IT could form the CB[8]/Im-Tpy/La^{3+} (CITL) assemblies with the carbonyl negative of the CB[8] port *via* ion-dipole interaction. As presented in Fig. S1 (Supporting information), the UV–vis absorption spectra of IT, the metal complex ITL and the supramolecular assemblies CITL were first examined. The UV–vis absorption spectra of the metal complex ITL showed a decrease in absorption at 275 nm compared to IT. When CB[8] was added, the UV absorption of CITL presented a red shift to 280 nm from 275 nm, in parallel with the appearance of a new absorption peak at 342 nm, which was caused by the intermolecular charge transfer interaction, evidencing that ITL entered the cavity of CB[8] and formed the CITL supramolecular assemblies.

The bonding mode of the host and guest molecules was analyzed by ^1H NMR, also as illustrated in Fig. 1A. When CB[8] was added to ITL, it can be seen that the proton signal peak had an obvious tendency to move to the low field and broaden, while the H_g and H_f proton signal peaks of the aromatic part both underwent a large high field shift, indicating that the aromatic part of IT has positioned in the CB[8] cavity, forming CITL supramolecular assemblies. The host-guest Job's plot curve determined the bonding ratio of the assemblies, as shown in Fig. 1C, the absorption change at 275 nm reached the maximum when the concentration molar ratio is 0.5 for CB[8]/CB[8]+[ITL], demonstrating that the bonding ratio of CB[8] to ITL was 1:1. In order to verify the stability of assemblies, the bonding constants of the assemblies were determined by UV titration experiments. CB[8] with different gradient concentrations from 0 to 0.025 mmol/L were added to 0.025 mmol/L ITL dropwise, and the UV–vis absorption spectra were measured at 25 °C. As shown in Figs. 1D and E, the bonding constant (K_s) of CITL was calculated to be 4.118×10^6 L/mol ($R^2 = 0.997$) by the nonlinear fitting method, and the above experiments indicated the good stability of the supramolecular assemblies. In addition, the zeta potentials of the assemblies were tested in Fig. S2 (Supporting information), CITL was $+2.16 \pm 0.26$ mV. Meanwhile, the zeta potentials at different time were measured, and found that the zeta potentials of CITL do not change significantly, which proved the excellent stability.

On the basis of the host-guest assembly model we hypothesized that CB[8] and ITL could form a continuous linear structure (Fig. 2A). The morphology of the assemblies was studied by transmission electron microscopy (TEM) and scanning electron microscopy (SEM). As revealed in Figs. 2B and C, the IT showed irregular particles with a size of about 40 nm. After coordination with rare-earth ions La^{3+}, TEM images of ITL showed stable and uniform spherical nanoparticles, which were approximately 60 nm in diameter on average (Figs. 2D and E). The addition of macrocyclic molecule CB[8] to ITL in a 1:1 stoichiometric ratio led to the disappearance of nanoparticles and the appearance of nanofibers with a diameter of about 20 nm, as shown in Figs. 2F and G. The above results indicated that CB[8] can be used as a "linker" for secondary assembly with ITL in an n:n bonding ratio to further aggregate and form supramolecular nanofibers.

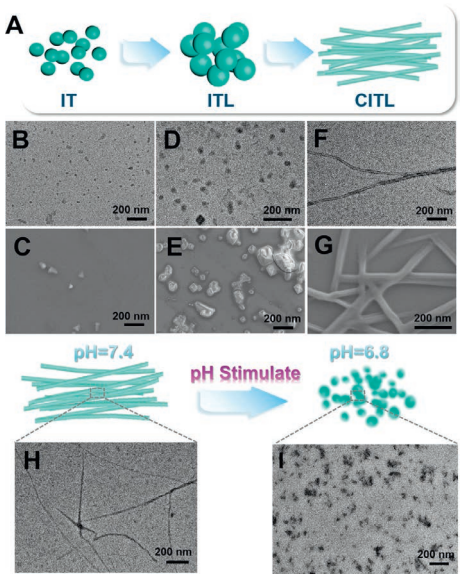


Fig. 2. (A) Schematic representation of morphological changes in supramolecular assemblies. TEM and SEM images of (B, C) IT, (D, E) ITL, (F, G) CITL. TEM images of CITL supramolecular nanofibers dissolved in (H) pH 7.4 PBS and in (I) pH 6.8 PBS (The concentration of different assemblies was 200 μmol/L).

Human organs and body fluids have their unique pH values, and cancer cells are surrounded by an acidic environment compared to normal cells, so we further investigated the morphological changes under acidic conditions. When the CITL was dissolved in pH 7.4 phosphate buffered saline (PBS), it remained as stable fibrous structures as shown in Fig. 2H. Further CITL was dissolved in pH 6.8 PBS as shown in Fig. 2I, and it can be found that the fibers-like structure disappeared and irregular nanoparticles around 50 nm appeared. Similarly, it is demonstrated by dynamic light scattering (DLS) that the hydrated ion radius of CITL decreased in pH 6.8 acidic condition (Fig. S3 in Supporting information). This is due to the strong host-guest interaction between CB[8] and ITL in a neutral environment, which made it easier for the guest to enter the cavity of the host and thus assemble into supramolecular nanofibers. However, in the acidic environment, the host-guest interaction weakened and the guest molecule ITL detached from the cavity of the host molecule CB[8], led to the disintegration of the nanofibers and a sudden decrease in size into irregular nanoparticles. This experiment demonstrated that the prepared one-dimensional supramolecular nanofibers possessed pH-sensitive deformation properties.

Supramolecular nanofibers exhibit potential lanthanide luminescence due to rare-earth ions doping. When excited at 290 nm, as shown in Fig. S4 (Supporting information), compared with CB[8]/Im-Tpy (CIT), CITL emitted a narrower and stronger blue fluorescence, it was the result of intramolecular energy transfer that occurred from the excited chelating ligand IT to La^{3+}. The fluorescence emission intensity of CITL gradually decreased as the excitation wavelength gradually increased from 290 to 320 nm to 370 nm (Fig. S5 in Supporting information). These results jointly indicated the excellent lanthanide luminescence behavior of supramolecular nanofibers, and also proved the existence of La^{3+} in the nanofibers.

Cancer cells produce a large amount of lactic acid through glycolysis and enhanced plasma membrane proton pump activity, resulting in a slightly acidic surrounding of cancer cells, it is clinically relevant to develop a smart nano drug delivery system with pH response. As shown in Fig. S6 (Supporting information), CITL supramolecular nanofibers synthesized by layer-by-layer self-

assembly have the properties of appropriate sizes, surface positivity and pH-sensitive deformation, which can be used as potential therapeutic drugs or carriers for tumors (Fig. S6A). Therefore, doxorubicin hydrochloride (Dox) was selected as a model drug to investigate the therapeutic effect on tumor enhancement. The drug loading behavior was first studied, as displayed in Fig. S6B, the Dox-loaded CITL (CITLD) showed a new absorption peak at 505 nm, which proved that Dox was successfully loaded. Compared with the absorption peak of Dox at 488 nm, the absorption peak of CITLD was red-shifted, which was caused by intermolecular π-π interactions. The drug encapsulation rate of CITL nanofibers was calculated to be 18.76% ± 1.13%. The TEM images of 200 μmol/L CITLD in pH 7.4 PBS demonstrated that the drug-loaded nanofibers had good dispersion and stability in neutral solutions (Fig. S6C).

The pH-sensitive drug release behavior of supramolecular nanofibers was further investigated. CITLD was dispersed in PBS with different pH values, and the drug release rate was determined by UV–vis spectrum under dark conditions. From Fig. S6D, the drug release of CITLD was limited in pH 7.4 PBS for the first 24 h, but a significant increase in Dox release was observed after adjusting pH to 6.0. Therefore, we further studied the pH dependence of drug release of drug-loaded nanofibers at different times. The drug release amounts of nanofibers at different pH were measured. As shown in Fig. S6E, the Dox release of CITLD was inhibited in pH 7.4 PBS solution, and the drug release was only 11.66% ± 0.81% after 96 h. However, under pH 6.8 PBS, drug release increased significantly, and the maximum drug release reached 76.15% ± 2.92%. With the gradual decrease of pH, when the pH value is 6.0, the release amounts of CITLD at 96 h were 90.02% ± 2.60%. Further lowering the pH to 5.0, the drug release rate was observed as high as 97.78% ± 3.04% after releasing 96 h. These results indicated that the CITLD drug delivery system had the properties of pH-dependent drug release behavior.

The drug release of supramolecular nanofibers was evaluated by changes in zeta potentials. As presented in Fig. S7 (Supporting information), the zeta potential of ITL is $+14.69 \pm 0.33$ mV, which decreased to $+1.66 \pm 0.37$ mV when combined with CB[8]. After loading drugs, the zeta potential decreased to -19.50 ± 0.24 mV, and the zeta potential changed little to -16.09 ± 0.32 mV after releasing in pH 7.4 PBS, indicating the low Dox release amount of CITLD. However, after releasing in pH 6.0 PBS solution, the zeta potential decreased sharply to -7.51 ± 0.41 mV, proving rapid drug release with pH response of CITLD. The reason for the above results may be that the tumor cells show acidic charges and bind to negatively charged fibers, possibly leading to enhanced cellular uptake.

In addition, the La^{3+} release ability of the drug-loaded supramolecular nanofibers was performed by inductively coupled plasma mass spectrometry (ICP-MS). As shown in Fig. S6F, the La^{3+} could be released consistently for 14 days, especially with a significant increase in a weakly acidic environment, where its concentration reached 273.51 μg/mL. It is due to that nanofibers decomposed and decreased in size under acidic conditions, stimulating effective drug release sequentially and quickly, which would play a potential role in cancer therapy.

The microenvironment of tumor cells and normal cells is quite different which is slightly acidic, so we chose different cells to explore the pH-sensitive anticancer properties of supramolecular nanofibers. As shown in Fig. 3A, cervical cancer cells (HeLa) were incubated with different assemblies for 24 h, and then the cell viability was measured by MTT assay. With the gradual increase in the concentration of the CITL and CITLD, the viability of HeLa cells was gradually reduced. At the concentration of 200 μmol/L, the cell viability was 49.88% ± 1.40% and 18.61% ± 2.71%, demonstrating the significant cytotoxicity of the assemblies to HeLa cells. To further explore the universality of supramolecular nanofibers to other tumor cells, human liver cancer cells (HepG2) and mouse-derived

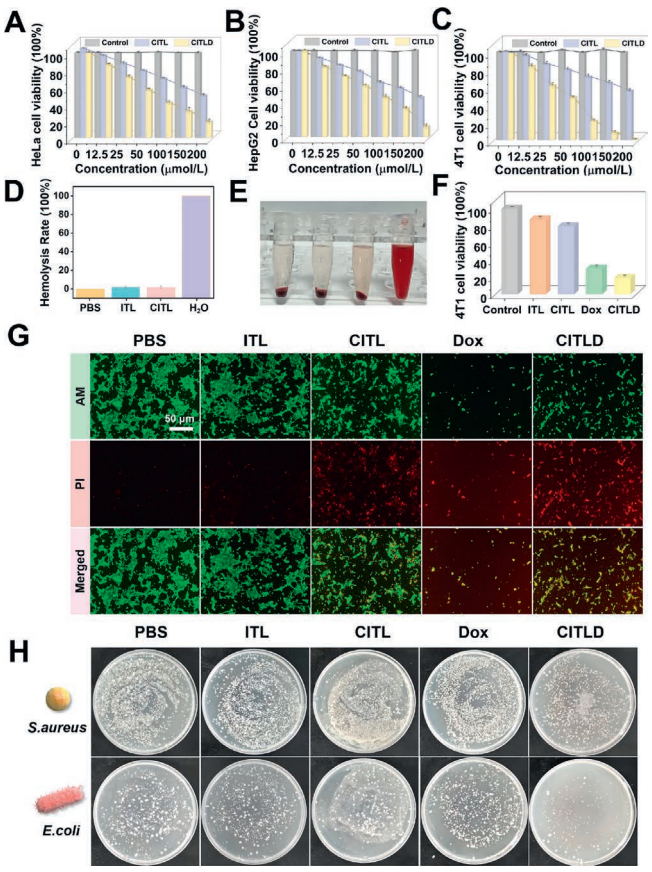


Fig. 3. Cytotoxicity of different concentrations of CITL and CITLD on (A) HeLa cells, (B) HepG2 cells, (C) 4T1 cells. (D, E) Hemolysis rate and digital photos of red blood cells with different assemblies. (F) The 4T1 cell viability of different assemblies at a concentration of 100 μmol/L. (G) Fluorescence images of calcein-AM/propidium iodide (PI) staining of 4T1 cells treated with different groups, the concentration of samples was 100 μmol/L. (H) Digital photos of different assemblies cultured for 12 h with *S. aureus* and *E. coli*, respectively. Data are presented as mean ± standard deviation (SD) ($n = 5$).

triple-negative breast cancer cells (4T1) were chosen for cytotoxicity determination. As displayed in Figs. 3B and C, the results showed that tumor cell survival still showed a decreasing trend. Interestingly, we found that the killing rate of 4T1 cells was 100% when the concentration of CITLD was 200 μmol/L. The above MTT experiments showed that the supramolecular drug-loaded system possessed a universal toxic effect on tumor cells.

To prove the tumor-specific toxicity of supramolecular nanofibers, human-derived normal liver cells (L02) and human umbilical vein endothelial cells (HUVEC) were selected as the control (Figs. S8 and S9 in Supporting information). With the gradual increase of CITL and CITLD, the cell viability of both were at a relatively high level. Even at a concentration of 200 μmol/L, the cell viability of L02 and HUVEC were greater than 80%. However, the L02 cell viability of drug-loaded supramolecular systems was lower than assemblies alone, which was due to the small amount of drug leakage from the system (Fig. S10 in Supporting information). Interestingly, we found that HUVEC showed greater drug sensitivity to Dox (Fig. S11 in Supporting information). The main reason why the nanofibers can selectively kill cancer cells with high specificity is due to their highly sensitive pH-responsive deformation characteristics. Also, the hemolysis test demonstrated the excellent biocompatibility of the assemblies (Figs. 3D and E). However, when cultured with 4T1, CITLD can rapidly release the Dox and kill the tumor cells (Figs. 3F and G). The above experimental results indicated that in the concentration range of

0–200 μmol/L, the supramolecular nanofibers had low biological toxicity to normal cells and high cytotoxicity to cancer cells, which could specifically and selectively kill cancer cells to reduce the side effects.

To investigate the uptake of nanofibers by tumor cells, 4T1 cells were cultured with CITLD at a concentration of 100 μmol/L for 0–3 h, and the nuclei were stained with 4′,6-diamidine-2-phenylindole dihydrochloride (DAPI). The bright field, DAPI staining, Dox fluorescence and merged pictures were shown from top to bottom in Fig. S12 (Supporting information), as the culture time from 1 h to 3 h gradually increased, the red fluorescence of Dox increased (Figs. S12G, K, O). Meanwhile, the distribution of red fluorescence also changed from cytoplasm to nucleus, as shown in Fig. S12P, indicating that drugs were successfully delivered into the nucleus. It was proved that the supramolecular nanofibers loaded with drugs were rapidly ingested through endocytosis and then effectively released in the tumor cells, thus it could take full effect and ultimately achieve the combination therapeutic effect.

The previous study found that bacteria are present in most tumors, which can render antibiotics or chemotherapy drugs ineffective, help tumors metastasize and resist treatment, thus the antibacterial effect of materials in cancer treatment should be considered. We selected Gram-positive bacteria *Staphylococcus aureus* (*S. aureus*) and Gram-negative bacteria *Escherichia coli* (*E. coli*) and cultured them with different assemblies for 12 h to investigate the antibacterial effects. As shown in Fig. 3H and Fig. S13 (Supporting information), it was evident that the bacterial numbers of both were reduced. The above experiment indicated that the supermolecular fibers we proposed not only directly exert antitumor effects but also have antibacterial functions, which have the potential to inhibit tumor metastasis and enhance treatment.

Subsequently, the anti-cancer effect of the supramolecular assembly was evaluated at the intracellular level. The animal experiments were carried out in strict accordance with internationally recognized standards and approved by the ethics application of the School of Pharmacy of Harbin Medical University (the ethics number: IRB3061723). The mice were randomly divided into five groups ($n = 5$) and the intratumor injection one time every day (Figs. 4A and B). Monitoring body weights of mice showed no significant changes indicating excellent biocompatibility of the materials (Fig. 4C). And the PBS, ITL and CITL treatment groups had a weak inhibitory effect on tumors, in contrast, tumors in mice treated with CITLD for 14 days were significantly reduced with an inhibition rate of 90.79% (Fig. 4D and Fig. S14 in Supporting information). It was consistent with the cell experiment results mentioned above, which further confirmed that CITLD possessed favorable anti-tumor properties. Tumors treated with different groups were further fixed and dissected for hematoxylin-eosin (H&E) staining and TdT-mediated dUTP nick-end labeling (TUNEL), both of which confirmed that the CITLD caused the most severe damage to the tumors and induced apoptosis of tumor cells (Fig. 4E). Moreover, there were no significant changes in the histology of major organs (heart, liver, spleen, lung and kidney) after 14 days of treatment in the different groups, and various blood analyses of the mice were shown to be within the normal range (Figs. S15 and S16 in Supporting information). Overall, these data suggested that CITLD treatment at a fixed dose was low-toxicity.

In summary, CITLD nanofibers were successfully synthesized based on supramolecular interaction, which had pH-sensitive deformation and antibacterial characteristics. It was found that layer-by-layer self-assembled nanofibers can effectively load anti-cancer drugs and achieve specific and sequential released Dox and La^{3+} in the TME, thereby achieving improved therapeutic efficacy. Meanwhile, the synergistic enhancement of therapeutic efficacy was achieved by reducing the excess of Gram-positive and Gram-negative bacteria surrounding 4T1 tumor cells. Due to nanofibers were constructed by small compounds based on supramolecular interaction, avoided metabolic problems caused by large molecule drugs, and showed excellent biocompatibility and safety. The simple and stable preparation of novel supramolecular nanofibers not only provides a novel synthetic route for drug carriers but also a potential platform for anti-tumor and other site-specific therapies.

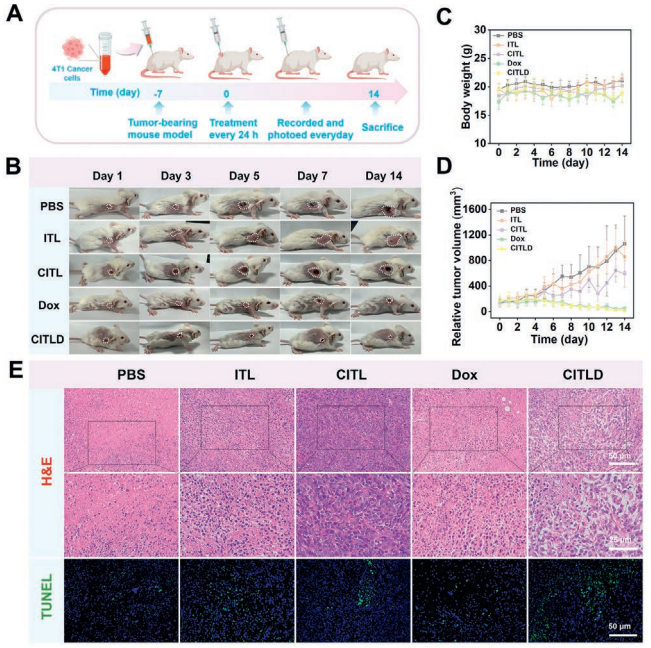


Fig. 4. (A) Schematic diagram of the construction of the tumor mouse model and treatment process. (B) Digital photos of 1, 3, 5, 7 and 14 days mice after different groups of treatments. Curves of (C) body weight and (D) relative tumor volume of mice after intratumoral injection of different assemblies. (E) H&E and TUNEL staining of tumor tissues from the different treatment groups. Data are presented as mean ± SD ($n = 5$).

Declaration of competing interest

The authors declare that they have no known competing financial interests or personal relationships that could have appeared to influence the work reported in this paper.

CRediT authorship contribution statement

Ting Zhang: Writing – review & editing, Writing – original draft, Supervision, Funding acquisition, Data curation, Conceptualization. **Deqiang Chen:** Writing – original draft, Investigation, Data curation. **Ningzhi Zhang:** Resources, Data curation. **Mingxu Zhang:** Software, Resources, Data curation. **Qiang Huang:** Validation, Data curation. **Wei Liu:** Investigation. **Ran Gao:** Formal analysis. **Yong Zhang:** Writing – review & editing, Funding acquisition.

Acknowledgments

This study was supported by the National Natural Science Foundation of China (No. 82273919), Natural Science Foundation of Heilongjiang Province (No. LH2024H013) and China Postdoctoral Science Foundation (No. 2022MD723781).

Supplementary materials

Supplementary material associated with this article can be found, in the online version, at doi:10.1016/j.cclet.2025.111117.

References

[1] X. Wang, X. Zhong, Z. Liu, L. Cheng, Nano Today 35 (2020) 100946.
[2] J. Chen, Y. Zhu, C. Wu, J. Shi, Chem. Soc. Rev. 49 (2020) 9057–9094.
[3] Z. Jing, Q. Du, X. Zhang, Y. Zhang, Chem. Eng. J. 446 (2022) 137147.
[4] G. Yang, Y. Liu, J. Chen, J. Ding, X. Chen, Acc. Mater. Res. 3 (2022) 1232–1247.
[5] S.L. Li, P. Jiang, F.L. Jiang, Y. Liu, Adv. Funct. Mater. 31 (2021) 2100243.
[6] K. Song, X. Su, W. Zhao, F. Ai, A. Umar, S. Baskoutas, Chem. Eng. J. 485 (2024) 150067.
[7] F.A.L.S. Silva, H.P. Chang, J.A.C. Incorvia, et al., Small 20 (2024) 2306137.
[8] X. Wu, Z. Zhou, K. Li, S. Liu, Adv. Sci. 11 (2024) 2308632.
[9] H. Han, H.A. Santos, Adv. Mater. 36 (2024) 2409522.
[10] C. Yu, L. Li, P. Hu, et al., Adv. Sci. 8 (2021) 2100540.
[11] X. Han, C. Saengow, L. Ju, et al., Nat. Commun. 15 (2024) 3435.
[12] Q. Li, Q. Song, Z. Zhao, et al., ACS Nano 17 (2023) 10376–10392.
[13] Z. Zhou, M. Vázquez-González, I. Willner, Chem. Soc. Rev. 50 (2021) 4541–4563.
[14] B. Hazarika, V. Singh, Chin. Chem. Lett. 34 (2023) 108220.
[15] T. Zhang, Y. Liu, B. Hu, et al., Chin. Chem. Lett. 30 (2019) 949–952.
[16] A. Feng, Y. Zhou, M.A.Y. Al-Shebami, et al., Nat. Chem. 14 (2022) 1158–1164.
[17] E. Mattia, S. Otto, Nat. Nanotechnol. 10 (2015) 111–119.
[18] D. Xu, Q. Zhou, X. Dai, et al., Chin. Chem. Lett. 33 (2022) 851–854.
[19] L. Zhou, C. Yang, W. Dou, et al., Chin. Chem. Lett. 35 (2024) 108669.
[20] S. Li, Y. Gao, Y. Ding, A. Xu, H. Tan, Chin. Chem. Lett. 32 (2021) 313–318.
[21] H. Fu, J. Huang, J.J.B. van der Tol, et al., Nature 626 (2024) 1011–1018.
[22] Z. Zhu, G. Zhang, B. Li, et al., Nat. Commun. 15 (2024) 8033.
[23] B. Wang, Y. Liu, X. Chen, et al., Chem. Soc. Rev. 53 (2024) 10189–10215.
[24] B. Mu, X. Hao, X. Luo, et al., Nat. Commun. 15 (2024) 903.
[25] Q. Yu, Y.M. Zhang, Y.H. Liu, et al., Sci. Adv. 4 (2018) e2297.
[26] S. Li, W. Zhang, R. Xing, et al., Adv. Mater. 33 (2021) 2100595.
[27] Y. Guo, P. Hu, J. Shi, J. Am. Chem. Soc. 146 (2024) 10217–10233.
[28] F.L. Locke, S. Filosto, J. Chou, et al., Nat. Med. 30 (2024) 507–518.
[29] C.F. Guerrero-Juarez, G.H. Lee, Y. Liu, et al., Sci. Adv. 8 (2022) eabn7981.
[30] X. Wang, H. Zha, W. Wu, et al., Sci. Transl. Med. 15 (2023) 5029.
[31] Y. Chao, Z. Liu, Nat. Rev. Bioeng. 1 (2023) 125–138.
[32] L. Li, M. Zhen, H. Wang, et al., Nano Today 48 (2023) 101702.
[33] L.A. Walsh, D.F. Quail, Nat. Immunol. 24 (2023) 1982–1993.
[34] D. Nejman, I. Livyatan, G. Fuks, et al., Science 368 (2020) 973–980.
[35] W.F. Song, D. Zheng, S.M. Zeng, et al., ACS Nano 16 (2022) 17402–17413.
[36] A. Fu, B. Yao, T. Dong, et al., Cell 185 (2022) 1356–1372.
[37] L.T. Geller, M. Barzily-Rokni, T. Danino, et al., Science 357 (2017) 1156–1160.
[38] B.P. Willing, S.L. Russell, B.B. Finlay, Nat. Rev. Microbiol. 9 (2011) 233–243.
[39] F. Klemm, J.A. Joyce, Trends Cell Biol. 25 (2015) 198–213.
[40] Y. Wang, Y. Han, C. Yang, et al., Nat. Commun. 15 (2024) 4194.